

pubs.acs.org/JPCB Article

Solubility Equilibrium Isotope Effects of Noble Gases in Water: Theory and Observations

Alan M. Seltzer,* Sarah A. Shackleton, and Ian C. Bourg



Cite This: https://doi.org/10.1021/acs.jpcb.3c05651



Read Online

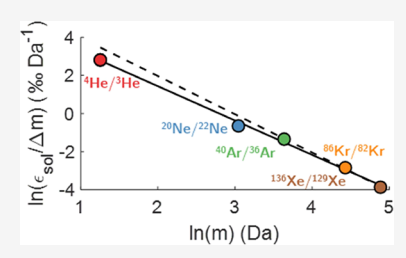
ACCESS I

Metrics & More

Article Recommendations

s Supporting Information

ABSTRACT: The abundance and isotopic composition of noble gases dissolved in water have many applications in the geosciences. In recent years, new analytical techniques have opened the door to the use of high-precision measurements of noble gas isotopes as tracers for groundwater hydrology, oceanography, mantle geochemistry, and paleoclimatology. These analytical advances have brought about new measurements of solubility equilibrium isotope effects (SEIEs) in water (i.e., the relative solubilities of noble gas isotopes) and their sensitivities to the temperature and salinity. Here, we carry out a suite of classical molecular dynamics (MD) simulations and employ the theoretical method of quantum correction to estimate SEIEs for comparison with experimental observations. We find that classical MD



simulations can accurately predict SEIEs for the isotopes of Ar, Kr, and Xe to order 0.01%, on the scale of analytical uncertainty. However, MD simulations consistently overpredict the SEIEs of Ne and He by up to 40% of observed values. We carry out sensitivity tests at different temperatures, salinities, and pressures and employ different sets of interatomic potential parameters and water models. For all noble gas isotopes, the TIP4P water model is found to reproduce observed SEIEs more accurately than the SPC/E and TIP4P/ice models. Classical MD simulations also accurately capture the sign and approximate magnitude of temperature and salinity sensitivities of SEIEs for heavy noble gases. We find that experimental and modeled SEIEs generally follow an inversesquare mass dependence, which implies that the mean-square force experienced by a noble gas atom within a solvation shell is similar for all noble gases. This inverse-square mass proportionality is nearly exact for Ar, Kr, and Xe isotopes, but He and Ne exhibit a slightly weaker mass dependence. We hypothesize that the apparent dichotomy between He-Ne and Ar-Kr-Xe SEIEs may result from atomic size differences, whereby the smaller noble gases are more likely to spontaneously fit within cavities of water without breaking water-water H-bonds, thereby experiencing softer collisions during translation within a solvation shell. We further speculate that the overprediction of simulated He and Ne SEIEs may result from the neglection of higher-order quantum corrections or the overly stiff representation of van der Waals repulsion by the widely used Lennard-Jones 6-12 potential model. We suggest that new measurements of SEIEs of heavy and light noble gases may represent a novel set of constraints with which to refine hydrophobic solvation theories and optimize the set of interatomic potential models used in MD simulations of water and noble gases.

1. INTRODUCTION

Dissolved noble gas isotopes are useful tracers in hydrology and oceanography due to their chemical and biological inertness. For example, dissolved helium isotope ratios in groundwater¹⁻⁴ and seawater⁵⁻⁸ have been used to determine water-mass residence times, quantify volcanic volatile inputs, and constrain physical and biogeochemical fluxes in the ocean. Recent analytical developments 9-11 for precise measurement of dissolved argon, krypton, and xenon isotope ratios in groundwater and seawater have enabled new applications for paleoclimate, ¹² groundwater hydrogeology, ¹³ and atmosphere—ocean gas exchange. ^{14,15} In addition to their broad applications in the geosciences, noble gas isotopes are also of fundamental interest to physical chemistry because of their inherent simplicity as inert, monatomic gases. For example, vapor-pressure isotope effects (VPIEs) of noble gases—i.e., the difference in vapor pressure between isotopes of the same noble gas-provide a useful means of evaluating physical models rooted in interatomic potential functions via

comparison to measurements of noble gas isotope fractionation. $^{16-19}\,$

In principle, solubility equilibrium isotope effects (SEIEs) of noble gases in water—i.e., differences in solubility between isotopes of the same noble gas—similarly provide insight into the physics of hydrophobic solvation as well as into the accuracy of water and noble gas interatomic potential functions.²⁰ Whereas SEIEs for polyatomic gases in fluids arise because of hindered translational, rotational, and internal vibrational frequencies of the gas molecule in solution,^{21,22} SEIEs of noble gases are governed purely by hindered

Revised: August 21, 2023 Revised: October 25, 2023 Accepted: October 30, 2023



translation^{20,23} because noble gases are monatomic. This simplicity makes noble gas SEIEs attractive for the evaluation of physical models. However, until recently, experimental constraints on noble gas SEIEs were known only for helium isotopes.^{24,25} Over the past decade, analytical advances have facilitated the determination of SEIEs for neon, argon, krypton, and xenon.^{11,26} Each of these noble gases displays a "normal isotope effect"²⁰ whereby the heavier isotope (e.g., ⁴⁰Ar) is more soluble than the lighter isotope (e.g., ³⁶Ar), as shown in Figure 1.

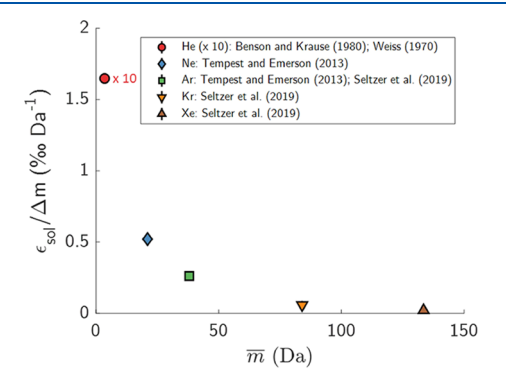


Figure 1. Experimentally determined solubility equilibrium isotope effects in freshwater from prior studies, $^{11,24-26}$ normalized by isotope-pair mass difference, as a function of the mean atomic mass of an isotope pair, \bar{m} (Da). Data are reported as ε values (where $\varepsilon \equiv \alpha - 1$), in $\%_o$, normalized by isotopic mass difference, Δm (Da). Note that analytical error bars are smaller than the symbols.

In this study, we explore the extent to which a classical molecular dynamics (MD) approach can accurately simulate SEIEs for the stable isotopes of noble gases. We closely follow the theoretical framework of Dang et al., 23 who employed classical MD to simulate SEIEs of He, N2, and Ar. To our knowledge, Dang et al. 23 made the first prediction of Ar isotopic solubility differences, several decades before the first experimental observations. Here, we carry out a suite of classical MD simulations for isotopes of He, Ne, Ar, Kr, and Xe in water at different temperatures, salinities, and pressures and with different water models and interatomic potential functions to compare simulated SEIEs with observations. We also report new high-precision measurements of the SEIEs for Ar isotopes in liquid water. We discuss our results in the context of the applicability of various water models and potential functions as well as the viability of classical MD simulations, with quantum corrections for translation, to simulate equilibrium isotope effects of monatomic gases.

2. THEORETICAL BASIS AND CLASSICAL MD SIMULATION APPROACH

Our study is concerned primarily with differences in the Henry solubility coefficient (H) of the heavy and light isotopes of noble gas. H is defined according to Henry's Law as

$$H \equiv C_{\text{diss}}/C_{\text{gas}}$$
 (1)

where $C_{\rm diss}$ and $C_{\rm gas}$ refer to dissolved and gas-phase concentrations of a noble gas isotope, respectively. We adopt conventional isotope geochemistry notation $(\alpha_{\rm sol})$ to refer to SEIEs, where $\alpha_{\rm sol}$ is an equilibrium fractionation factor representing the ratio of heavy-to-light isotope ratios in the dissolved and gas phases, respectively, at solubility equilibrium:

$$\alpha_{\text{sol}} = \frac{\left(\frac{C_{\text{h}}}{C_{\text{l}}}\right)_{\text{diss}}}{\left(\frac{C_{\text{h}}}{C_{\text{l}}}\right)_{\text{gas}}} = H_{\text{h}}/H_{\text{l}}$$
(2)

In eq 2, and hereafter, the subscripts h and l refer to heavy and light isotopes of noble gas, respectively.

Following Dang et al.,²³ and based upon Bigeleisen–Meyer theory,²² equilibrium isotope effects are equal to the ratio of reduced isotopic partition function ratios between dissolved and gas phases:

$$\alpha_{\text{sol}} = \frac{(s_{\text{h}}/s_{\text{l}})f_{\text{diss}}}{(s_{\text{h}}/s_{\text{l}})f_{\text{gas}}}$$
(3)

The reduced isotopic partition function ratio in the gas phase, (s_h/s_l) $f_{\rm gas}$, is unity for isotopes of a monatomic gas, while the reduced isotopic partition function in the dissolved phase, (s_h/s_l) $f_{\rm diss}$, is derived from the method of quantum correction for translational degrees of freedom. Here, as in Dang et al., ²³ we adopt the first quantum correction, yielding the following relationship between isotopic solubility differences, $\alpha_{\rm sol}$, and the mean square force experienced by the noble gas atom, $\langle (F)^2 \rangle$, which can be estimated using classical MD simulations and is independent of isotopic mass:

$$\alpha_{\text{sol}} = (s_{\text{h}}/s_{\text{l}}) f_{\text{diss}} = 1 + \frac{\hbar^2}{24(kT)^3} (\frac{1}{m_{\text{l}}} - \frac{1}{m_{\text{h}}}) \langle (F)^2 \rangle$$
 (4)

In eq 4, m refers to isotopic mass in Da, \hbar is the reduced Planck constant (1.054572 × 10³⁴ J s), k is the Boltzmann constant (1.380658 × 10⁻²³ J K⁻¹), and T is absolute temperature.

To illustrate how this framework allows for the estimation of SEIEs via classical MD simulation, we consider the example of Ar isotopes in freshwater at 298 K. For this example, we carried out five separate simulations (see Section 3 for a detailed description) each with an Ar atom of varying mass (either 4, 23, 40, 53, or 132 Da) surrounded by 1000 water molecules, using the software LAMMPS.²⁷ We represent water-water interatomic interactions using the SPC/E water model²⁸ and noble gas—water interactions with a Lennard-Jones 6–12 model (using the parameter values of ref 29). This set of interatomic potential models has been extensively validated against experimental results on the structure and dynamics of liquid water^{30,31} and on the solvation structure, solubility, and self-diffusion coefficients of noble gases in liquid water.^{29,32} Each simulation was equilibrated in the isothermal-isobaric (NPT) ensemble at 298 K and 1 bar (see Section 3) and then simulated for 25 ns in the canonical (NVT) ensemble with a 1

For each simulation, the mean squared translational force, $\langle (F)^2 \rangle$, is determined by evaluating the curvature of the normalized velocity autocorrelation function (VACF) of the noble gas atom at time t=0. We calculate the normalized VACF as

$$c(t) = \frac{\langle V(t) \cdot V(0) \rangle}{\langle V^2(0) \rangle} \tag{5}$$

where V(t) is the instantaneous velocity in any direction at simulation time t. We split each 25 ns simulation into 100 equal-time (250 ps) segments, and within each segment, we compute the average VACF over 3 ps intervals, averaging

across x, y, and z dimensions. As an example, Figure 2 shows the mean VACF, prior to normalization, evaluated across each

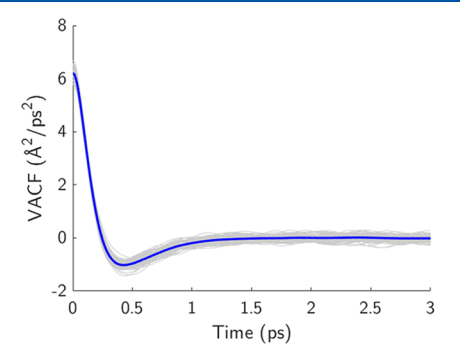


Figure 2. Velocity autocorrelation function (VACF) for 40 Ar in pure liquid water at 298 K averaged over the x, y, and z directions. The thick blue line represents the mean VACF over the entire 25 ns simulation, and the thin gray lines represent mean VACF values across one hundred 250 ps-long subsegments.

of the 100 segments (thin gray lines) and averaged over the entire simulation (thick blue line) for $^{40}\mathrm{Ar}$ in pure water at 298 K

The normalized VACF may be used to calculate the mean square translational force experienced by the noble gas by taking the second-order Taylor expansion and applying the equipartition theorem (see ref 23), which yields the following relation:

$$c(t) = 1 - \frac{\left(\frac{t^2}{2}\right)\langle (F)^2 \rangle}{3mkT} \tag{6}$$

Ultimately, eq 6 can be converted to a relation between the second derivative of the normalized VACF at t=0, and the mean square force $\langle (F)^2 \rangle$, which can then be used to determine a translational Einstein frequency, $\nu_{\rm et}$:

$$\nu_{\rm et} = \sqrt{-\frac{d^2(c(t=0))}{dt^2}} / (2\pi c)$$
 (7)

where variable c in the denominator is the speed of light. Finally, values of $\nu_{\rm et}$ determined for a pair of isotopes of different mass using eq 7 can be substituted into the relation between $\nu_{\rm et}$ and $\langle (F)^2 \rangle$, eq 4, to determine the solubility equilibrium fractionation factor between the two isotopes:

$$\alpha_{\text{sol}} = (s_{\text{h}}/s_{\text{l}})f_{\text{gas}} = 1 + \frac{\hbar^2}{8(kT)^2}(\nu_{\text{et,l}}^2 - \nu_{\text{et,h}}^2)$$
 (8)

We refer the reader to Dang et al. ²³ for further details and discussion of this derivation. We emphasize that the relative simplicity of eq 8 is inherently tied to the monatomic nature of the solute. For multiatomic solutes, $\alpha_{\rm sol}$ also depends on contributions associated with solute rotations and intramolecular vibrations, such that eq 8 becomes significantly more complex. ^{21,22}

In practice, we use a wide range of noble gas isotopic masses to obtain better statistical precision on the mass dependence of $\nu_{\rm et}$. In other words, we estimate the function $\nu_{\rm et}(m)$ by linear regression of $\ln(\nu_{\rm et})$ against $\ln(m)$ using values of $\nu_{\rm et}$ determined via simulations carried out at five real or hypothetical noble gas isotopic masses. We then evaluate this function at the masses of the existing stable noble gas isotopes.

Figure 3 shows an example of Ar isotopes in water at 298 K, evaluated at Ar isotope masses of 36, 38, and 40 Da (green

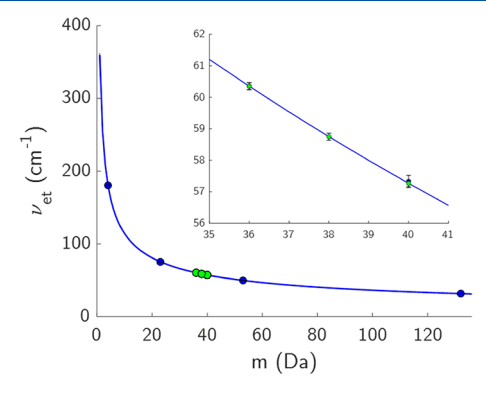


Figure 3. Translational Einstein frequency ($\nu_{\rm et}$) as a function of isotopic mass for Ar in freshwater at 298 K. Blue circles represent $\nu_{\rm et}$ values obtained from individual 25 ns MD simulations carried out at Ar isotopic masses of 4, 23, 40, 53, and 132 Da, and the blue line is a line of best fit [linear fit of $\ln(\nu_{\rm et})$ vs $\ln(m)$]. Inset: fitted curve evaluated at stable Ar isotope masses of 36, 38, and 40 Da (green circles) for the purpose of determining fractionation factors via eq 8.

symbols) based on MD simulations carried out at Ar isotope masses of 4, 23, 40, 53, and 132 Da (blue symbols). With estimates of $\nu_{\rm et}$ for $^{40}{\rm Ar}$ and $^{36}{\rm Ar}$ and using eq 8, we find a mean $\alpha_{\rm sol}$ value of 1.001057 ($\varepsilon_{\rm sol}=1.058\%$), which is close to observations of $\varepsilon_{\rm sol}$ for $^{40}{\rm Ar}/^{36}{\rm Ar}$ in freshwater at 293 to 298 K (1.012 \pm 0.012% at 298 K from ref 11; 1.04 \pm 0.05% at 293 K from ref 26). The statistical uncertainty on our estimate is negligible (\sim 0.0002% o) owing to the length of the simulations, but it is prone to systematic bias due to the choice of model parameters (i.e., water—water and noble gas—water interatomic potentials models). Quantifying these biases is the purpose of the sensitivity tests we carry out in this study (Section 3). We also note that the $\ln(\nu_{\rm et})$ vs $\ln(m)$ linear fitting approach is rooted in the physical expectation that the rattling frequency of a gas within a solvation shell should vary with the inverse square root of the mass of the gas for a simple harmonic oscillator. Our linear fit does not impose a slope of -0.5.

Notably, the simulated and experimental $\alpha_{\rm sol}$ values listed above for $^{40}{\rm Ar}$ and $^{36}{\rm Ar}$ agree within a factor of 2 with the 34-year-old simulation prediction of Dang et al., 23 who suggested a value of 1.0017 based on a 1.25 ps-long simulation with 192 water molecules. Although Dang et al. 23 did not report a statistical uncertainty, we suspect that the deviation of their value from our simulation and recent experimental constraints is primarily attributable to the three orders-of-magnitude shorter simulation time due to computational limitations of that era. Our only substantive advance, therefore, is simply the application of their theoretical framework to a set of new and much longer classical MD simulations. In doing so, we find astonishingly close agreement with experimental data, not only for Ar isotopes but also for isotopes of other noble gases, as described in detail in the remainder of the paper.

3. METHODS

3.1. MD Simulations. We carried out a total of 12 series of classical MD simulations (Table 1) to evaluate SEIEs of noble gas isotopes in water under different temperature, salinity, and pressure conditions and to test the sensitivity of these results to the choice of Lennard-Jones 6–12 parameters, water model,

Table 1. Overview of the Features That Were Varied in the 12 Series of MD Simulations

	freshwater control		saltwater tests		pressure tests		rigid test	LJ test	TIP4P model		TIP4P/ice model	
temperature (K)	298	278	298	298	298	298	298	298	298	278	298	278
salinity (g/kg)	0	0	35	115	0	0	0	0	0	0	0	0
pressure (bar)	1	1	1	1	-100	100	1	1	1	1	1	1
water model	а	а	а	а	а	а	а	а	b	b	с	c
noble gas LJ parameters	B08	B08	B08	B08	B08	B08	B08	W15	B08	B08	B08	B08
run time (ns)	25	25	25	25	5	5	5	25	5	5	5	5
rigid H ₂ O?	No	No	No	No	No	No	Yes	No	No	No	No	No
simulation series #	1	2	3	4	5	6	7	8	9	10	11	12

[&]quot;Water models are labeled a (SPC/E²⁸), b (TIP4P³³), or c (TIP4P/ice³⁴). The two sets of noble gas—water Lennard-Jones 6–12 parameters employed are referred to as B08 (ref 29 and W15 (ref 35).

Table 2. Compilation of Noble Gas SEIEs in Water from Prior Experimental Work 11,14,24,26 and New Measurements Made in This Study a

ratio	$arepsilon_{ m sol}$ (293,0) (% $_{o}$)	a (%o K ⁻¹)	$b \ (\% e \ \text{kg g}^{-1})$	Δm (Da)	reference
⁴ He/ ³ He	16.6	-0.088	0.008	0.9866	ref 24
22 Ne/ 20 Ne	1.04	n/a	n/a	1.9989	ref 26
40 Ar/ 36 Ar	1.041	-0.0072	0.0009	3.9948	this study
38 Ar/ 36 Ar	0.548	-0.0037	0.0004	1.9952	this study
$^{86}{ m Kr}/^{82}{ m Kr}$	0.232	-0.0008	0.0002	3.9971	refs 11,14
$^{86}{ m Kr}/^{83}{ m Kr}$	0.167	-0.0007	0.0004	2.9965	refs 11,14
$^{86}{ m Kr}/^{84}{ m Kr}$	0.115	-0.0007	-0.0001	1.9991	refs 11,14
136 Xe/ 129 Xe	0.145	-0.0014	0.0003	7.0024	refs 11,14
134 Xe/ 129 Xe	0.117	0.0003	0.0004	5.0006	refs 11,14
132 Xe/ 129 Xe	0.067	0.0001	0.0001	2.9994	refs 11,14

 $[^]ae_{sol}(293,0)$, a, and b, refer to the 293 K isotope effect and temperature and salinity dependences, respectively. The isotopic mass difference associated with each ratio, Δm , is given in Da, along with the reference for each set of SEIE values.

and treatment of water molecules as rigid bodies. For each series (i.e., for each column in Table 1), 25 separate classical MD simulations were run for five prescribed masses of helium (1, 4, 7, 20, 40 Da), neon (4, 20, 34, 84, 132 Da), argon (4, 24, 40, 53, 132 Da), krypton (4, 69, 84, 99, 132 Da), and xenon (4, 40, 84, 119, 132 Da). Each simulation was initialized with a single noble gas atom surrounded by 1000 water molecules in a cubic cell with periodic boundary conditions. Simulations were first initialized at the desired temperature and a constant volume $(30 \times 30 \times 30 \text{ Å})$, i.e., in the canonical (NVT) ensemble, for 20 ps. Next, the system was equilibrated for 80 ps at a constant pressure (1 bar) at the desired temperature in the isothermal-isobaric (NPT) ensemble. Following this, the average cell dimensions from the constant pressure equilibration were adopted, and the simulation was equilibrated for an additional 150 ps in the NVT ensemble. Finally, the simulations were carried out for 5-25 ns in the NVT ensemble, as shown in Table 1. This equilibration process was repeated separately for each noble gas and in each simulation series. Depending on the series (Table 1), the SPC/ E, 28 TIP4P, 33 or TIP4P/ice 34 models were used to represent water molecules. Noble gas-O interatomic interactions²⁸ were represented using the Lennard-Jones (LJ) 6–12 model:

$$\phi(r) = 4\epsilon \left[\left(\frac{\sigma}{r} \right)^6 - \left(\frac{\sigma}{r} \right)^{12} \right] \tag{9}$$

where ϕ is the interatomic potential (kJ mol⁻¹), r is the interatomic distance (Å), $2^{1/6}\sigma$ is the distance (Å) of the potential well, and ε is the depth of the potential well (kJ mol⁻¹). Depending on the series, we used one of two sets of published LJ parameter values^{29,35} for noble gas—water potentials. Simulations were carried out with the LAMMPS

software 27 using Verlet integration of Newton's equations of motion 36 to calculate molecular trajectories at 1 fs resolution. As described in the example presented in Section 2, VACFs were determined from the instantaneous velocities of noble gas atoms in each of these simulations such that eqs 5–8 could be used to calculate $\alpha_{\rm sol}$ values for isotopes of He, Ne, Ar, Kr, and Xe by evaluating fitted mass-dependence curves of $\nu_{\rm et}$ at actual isotopic masses (e.g., 22 and 20 Da, for Ne). To evaluate the influence of salinity, two "saltwater" simulation series were carried out at NaCl concentrations of 35 or 115 g kg $^{-1}$ and implemented using the NaCl model of Smith and Dang. 37 In these saltwater simulations, Na–O and Cl–O interatomic interactions were represented using the LJ 6–12 parameters of Smith and Dang, 37 and Na-noble gas and Cl-noble gas interaction parameters were calculated via Lorentz–Berthelot mixing rules.

3.2. Experimental SEIE Determinations. Air-water equilibration experiments were carried out in the Seltzer Lab at Woods Hole Oceanographic Institution (Woods Hole, MA) to redetermine SEIEs and their temperature and salinity dependences for the stable isotopes of Ar. In total, 46 new measurements were made using a recently developed airwater equilibration system that was used in a separate recent study to redetermine the bulk elemental solubilities of the noble gases in water.³⁸ In this study, experiments were carried out at temperatures between ~275 and 296 K and salinities between 0 and \sim 33 g kg⁻¹. A new technique for high-precision dynamic mass spectrometry measurements of dissolved noble gas isotopes in water was used^{9,10} in which evacuated 6-L stainless steel flasks were filled part way (~2 to 4 L of water), equilibrated on a shaker table at constant temperature (~295 K) for a minimum of 3 days, and drained to remove

Table 3. Summary of SEIE Results from the 12 Classical MD Simulation Series Described in Table 1 (Columns Labeled #1 through 12), Reported as ε_{sol} Values in %

ratio	# 1	# 2	# 3	# 4	# 5	# 6	# 7	# 8	# 9	# 10	# 11	# 12
⁴ He/ ³ He	20.16	22.63	20.77	21.45	20.53	19.58	19.57	20.65	19.51	22.25	22.46	24.39
22 Ne/ 20 Ne	1.306	1.499	1.334	1.413	1.328	1.281	1.283	1.322	1.281	1.454	1.453	1.616
40 Ar/ 36 Ar	1.058	1.214	1.077	1.116	1.074	1.037	1.051	1.158	1.027	1.189	1.207	1.332
38 Ar/ 36 Ar	0.557	0.639	0.567	0.587	0.565	0.546	0.553	0.609	0.541	0.626	0.635	0.701
86 Kr/ 82 Kr	0.233	0.265	0.238	0.250	0.238	0.231	0.231	0.254	0.226	0.258	0.267	0.290
86 Kr/ 83 Kr	0.173	0.196	0.176	0.185	0.176	0.171	0.171	0.188	0.167	0.191	0.198	0.215
$^{86}{ m Kr}/^{84}{ m Kr}$	0.114	0.129	0.116	0.122	0.116	0.113	0.113	0.124	0.110	0.126	0.130	0.142
136 Xe $/^{129}$ Xe	0.177	0.202	0.182	0.187	0.143	0.138	0.174	0.195	0.171	0.200	0.202	0.226
$^{134}{ m Xe}/^{129}{ m Xe}$	0.129	0.147	0.132	0.135	0.103	0.100	0.126	0.141	0.124	0.145	0.147	0.164
$^{132}{ m Xe}/^{129}{ m Xe}$	0.078	0.089	0.080	0.082	0.063	0.061	0.077	0.086	0.076	0.088	0.089	0.100

equilibrated water, leaving behind the headspace gas and a small (quantified) residual amount of water. The headspace gas was purified by exposure to a chemical getter (Ti sponge) at 900 °C and cryogenically transferred to a Thermo MAT 253 Plus mass spectrometer using a silica gel-containing dual-valve dip tube as an intermediary, following the method of ref 10. Small corrections were made for the noble gases contained in drained and residual water, following ref 9. Although isotopes of Ar, Kr, and Xe, in addition to Kr/Ar and Xe/Ar elemental ratios, were measured, here we report only Ar isotope ratios (40Ar/36Ar and 38Ar/36Ar) due to the fact that Kr and Xe isotope and elemental ratios in water are used to constrain instrumental matrix effects in this method, and thus our measured values are implicitly tied to published values for Kr and Xe SEIEs. 11,14 Our new Ar isotope measurements are made entirely independently of prior studies and thus provide an opportunity to comprehensively redetermine SEIEs.

Table 2 provides a summary of published and new experimental determinations of noble gas SEIEs. We report SEIEs as $\varepsilon_{\rm sol}$ values ($\varepsilon_{\rm sol} \equiv \alpha_{\rm sol} - 1$) in $\%_o$ in Table 2, and temperature and salinity dependences are treated linearly, such that

$$\varepsilon_{\text{sol}}(T, S) = \varepsilon_{\text{sol}}(293, 0) + a(T - 293) + bS$$
 (10)

where T is water temperature (K), S is salinity (g kg $^{-1}$), and ε_{293} is the $\varepsilon_{\rm sol}$ value at 293 K in freshwater. We note that the published helium isotope SEIE function is quadratic in form, 24 but that our linear approximation is accurate to within $\sim 0.1\% o$ (between 273 and 298 K and 0-100 g kg $^{-1}$), which is well below the precision of noble gas mass spectrometry for dissolved helium isotopes in water. The temperature and salinity dependences of neon isotope SEIEs are not presently known, but the freshwater value at 293 K has been experimentally determined.

4. RESULTS

Table 3 contains a summary of results ($\varepsilon_{\rm sol}$ values) from the 12 series of classical MD experiments carried out in this study. For each series, SEIEs are reported for each noble gas isotope ratio considered in this study (i.e., those listed in Table 2). For convenience, we also report these same results as percent differences from the results of Series 1 (the base case) in Table S1. Below, we discuss these findings and compare freshwater and saltwater MD-derived SEIEs to experimental observations.

4.1. Pure Water Simulations. Figure 4 shows a compilation of SEIEs ($\varepsilon_{\rm sol}$ values) determined via MD simulations and experimental measurements between 278

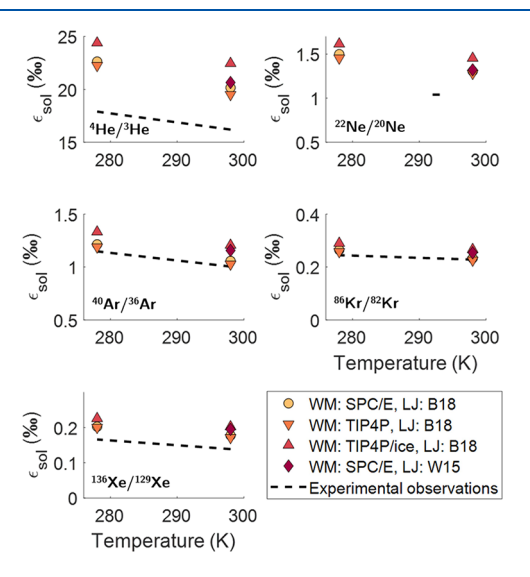


Figure 4. Comparison of simulated and experimentally observed SEIEs for isotope ratios of helium, neon, argon, krypton, and xenon in freshwater between 278 and 298 K. Marker symbols refer to experiments run with different water models (WM) or noble gas—water Lennard-Jones interaction parameters (LJ), as listed in Table 1. $\varepsilon_{\rm sol}$ values from MD simulations were calculated following the method outlined inSection 2 (i.e., eqs 5–8). Experimentally observed $\varepsilon_{\rm sol}$ values come from Table 2.

and 298 K in pure water. Overall, independent of the water model or solute-water interatomic potential functions used, all MD simulations broadly reproduce the relative magnitude of experimentally determined SEIEs (i.e., Figure 1), where isotope effects (normalized by Δm) monotonically decrease in magnitude as elemental mass increases such that isotope effects are largest for He and smallest for Xe. Across the three water models used (Table 1), we find the closest agreement between simulated and observed SEIEs when the TIP4P water model is employed for all five noble gases considered in this study. We generally observe the poorest simulation-observation agreement for the TIP4P/ice model. The sensitivity of simulated SEIEs to the choice of water model or gas-water interatomic potential parameters is generally small. For example, the largest observed deviation between predictions obtained with different interaction potentials (at 298 K) is 2.95% for ⁴He/³He at 298 K (Tables 3 and S1), representing a range of less than 20% of the observed magnitude of the SEIE (16.2%). We find that the sensitivities of SEIEs to pressure and the treatment of water molecules as rigid bodies (i.e., comparison of Experiments 1 and 7) are negligible for all

noble gas isotopes considered in this study, in both an absolute and relative sense (Figure S1, Table S1).

We find the closest agreement between simulations and observations for the isotopes Ar, Kr, and Xe. For the bestperforming water model (TIP4P; series #9 and #10), simulated $\varepsilon_{\rm sol}$ values agree with observations at 278 and 298 K to within 0.041% for isotope ratios 40Ar/36Ar, 86Kr/82Kr, and 136 Xe/ 129 Xe (Table 3), which is on the same order as the analytical uncertainty. 10,11 For the isotopes of He and Ne, we find poorer overall agreement, with simulations consistently overpredicting mean-square forces acting on He and Ne atoms and thus overestimating the magnitude of SEIEs (Figure 4). Nonetheless, even for He and Ne, the poorest simulationobservation agreement is still within 40% of the experimentally observed value for each simulation shown in 4. Note that experimental errors are quite small, on the orders of 0.1% for 4 He/ 3 He (ref 24) and 0.001–0.01‰ for Ne, Ar, Kr, and Xe isotopes (refs 11,14,26). The sensitivity of SEIEs to the choice of noble gas-water Lennard-Jones 6-12 parameters is in all cases smaller than the sensitivity to the choice of water model (Table 3, Table S1). Simulations carried out with the Warr et al. Lennard-Jones 6–12 parameters (series # 8) yield $\varepsilon_{\rm sol}$ values slightly higher (up to 10%) than those carried out using the Bourg et al.²⁹ parameters and using the same SPC/E water model (Tables 3 and S1).

We find that magnitudes of simulated SEIEs decrease with increasing temperature for all noble gas isotopes, based on series of 278 and 298 K simulations carried out with three different water models (Figure 4, Table 3; series #1-2, 9-10, and 11-12). Experimentally determined He, Ar, Kr, and Xe SEIEs similarly display a clear anticorrelation with temperature (Table S2, Figure 4), while no experimental determinations of the temperature dependence of the Ne SEIEs exist. Although the temperature dependence of experimentally determined SEIEs is well approximated as linear (e.g., eq 10), we note that eq 8 suggests an inverse-square temperature dependence, provided that all other variables in eq 8 are insensitive to temperature. Over the small range of temperatures for which experimental data exist (\sim 275-298 K), we find that experimentally determined and simulated SEIEs are similarly well described by an inverse-square temperature dependence (Figure S2). Further, as a sensitivity test, we calculated SEIEs by holding T constant (at 298 K) in eq 8. We find that the temperature dependences of SEIEs calculated with a constant T value in eq 8 are substantially reduced. For example, the mean difference in magnitude of simulated $\varepsilon_{\rm sol}$ values for ³He/⁴He between 278 and 298 K (averaged across the three different water models) was $2.38 \pm 0.41\%$ (1σ) without holding T fixed in eq 8, but it was reduced to $-0.61 \pm 0.54 \%$ (1σ) with T fixed at 298 K. This implies that the mean-square force acting on a noble gas atom is very weakly dependent on temperature and suggests that the observed anticorrelation between SEIE magnitude and temperature is dominated by the inverse-square temperature dependence of eq 8. For the remainder of this section, we focus on the isotopes of Ar, Kr, and Xe, for which simulations closely match the magnitude and temperature dependence of recent high-precision observations.

Consideration of Ar, Kr, and Xe isotopes also provides a unique opportunity to consider the mass dependence of SEIEs (i.e., the dependence of $\varepsilon_{\rm sol}$ on isotopic mass difference, Δm), because precise experimental determinations of SEIEs have now been made for multiple isotopes of each of these gases

(Table 2). One peculiar aspect of SEIEs in freshwater noted by ref 11 is the nonlinear mass proportionality of SEIEs for Ar isotopes but linear mass proportionality of SEIEs for Kr and Xe isotopes. For example, the experimentally determined 293 K $\varepsilon_{\rm sol}$ value for $^{38}{\rm Ar}/^{36}{\rm Ar}$ is $0.548 \pm 0.004\%$, which is more than half the value for $^{40}{\rm Ar}/^{36}{\rm Ar}$ ($1.041 \pm 0.004\%$), despite the fact that the isotopic mass difference of $^{38}{\rm Ar}/^{36}{\rm Ar}$ ($\Delta m = 2$) is half that of $^{40}{\rm Ar}/^{36}{\rm Ar}$ ($\Delta m = 4$; Table 2). However, the experimentally determined SEIE magnitude for $^{86}{\rm Kr}/^{84}{\rm Kr}$ ($0.115 \pm 0.009\%$; $\Delta m = 2$) is exactly half that of $^{86}{\rm Kr}/^{82}{\rm Kr}$ ($0.232 \pm 0.014\%$; $\Delta m = 4$), within analytical error (Table 2). As shown in Figure 5, we find that the mass proportionality (or

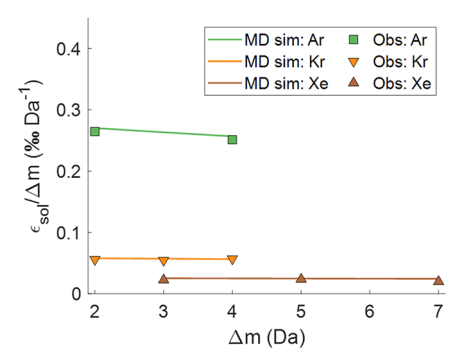


Figure 5. Comparison of the mass dependence of SEIEs for argon, krypton, and xenon isotopes in classical MD simulations (lines) and experimental observations (symbols). Observed values are from Table 2 (at 298 K via eq 10). Shown here are simulated values using the TIP4P water model at 298 K, where the fitted mass curve of $\nu_{\rm et}$ is evaluated at the isotopic masses of the isotope ratios reported in Table 2 and $\varepsilon_{\rm sol}$ values are computed via eq 8. Note that the linear dependence of $\varepsilon_{\rm sol}$ on the isotopic mass difference should appear as a horizontal line on this plot, consistent with simulations and observations for krypton and xenon isotopes. For Ar isotopes, the nonlinearity of $\varepsilon_{\rm sol}$ as a function of isotopic mass difference is apparent in both simulations and observations.

lack thereof) suggested by classical MD simulations matches the experimentally observed mass proportionalities. Mechanistically, we can understand these differences in mass proportionality as a function of the steepness of the $\nu_{\rm et}$ vs m curve (e.g., Figure 3). In the mass range of argon isotopes, this logarithmic curve is substantially steeper than those in the mass range of krypton and xenon isotopes. Thus, via eq 8, we find a greater SEIE magnitude (per isotopic mass difference) for Ar isotope ratios with a lighter mean isotopic mass (i.e., a greater magnitude for $^{38}{\rm Ar}/^{36}{\rm Ar}$ than for $^{40}{\rm Ar}/^{36}{\rm Ar}$). While no experimental observations exist for SEIEs containing $^{21}{\rm Ne}$, we can predict that the SEIE for $^{21}{\rm Ne}/^{20}{\rm Ne}$ will be more than twice as large as that for $^{22}{\rm Ne}/^{20}{\rm Ne}$, since Ne isotopes lie within an even steeper portion of the $\nu_{\rm et}$ curve than do Ar isotopes.

4.2. Saltwater Simulations. Most dissolved gases, including the noble gases, ^{38,39} exhibit a Setschenow "salting out" effect, whereby the bulk (molecular) solubility of the gas in liquid water decreases with increasing solution ionic strength. ⁴⁰ Until recently, it was unknown to what extent salinity might impact the relative solubility of noble gas isotopes (i.e., the magnitude of SEIEs), except for the ⁴He/³He ratio of dissolved He, which exhibits a slight increase in the magnitude of its SEIE with increasing salinity ^{24,25} (e.g., an increase in $\varepsilon_{\rm sol}$ of ~0.2% in seawater relative to freshwater). More recently, experimental determinations of Ar, Kr, and Xe

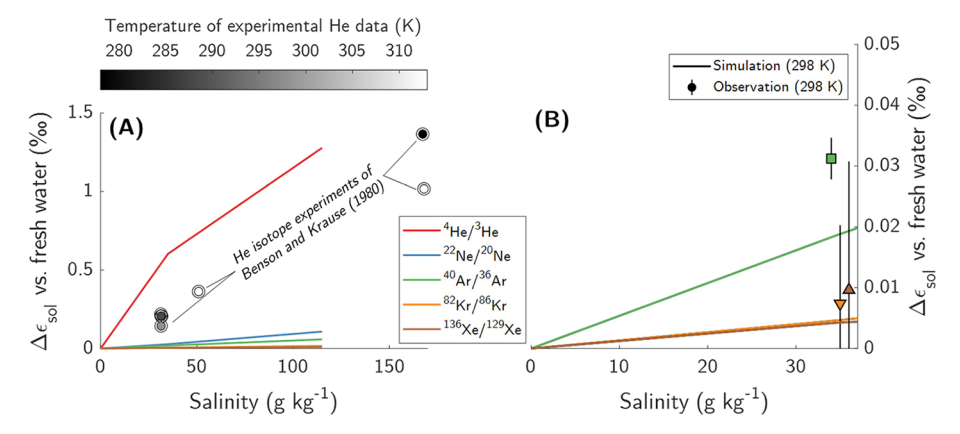


Figure 6. Salinity dependence of helium, neon, argon, krypton, and xenon SEIEs. Results from MD simulation experiments carried out at salinities of 0, 35, and 115 g kg⁻¹ are shown in panel (A), where salinity effects are reported as deviations $\Delta \varepsilon_{\rm sol}$ between the magnitude of fractionation at given salinity and in freshwater at 298 K. As listed in Table 1, these simulations were carried out using the SPC/E water model with Bourg and Sposito²⁹ and Smith and Dang²⁹ interatomic potentials for noble gases and NaCl, respectively, at a pressure of 1 bar and treating water molecules as flexible. Also shown (colored circles) are observationally constrained He SEIE salinity effects from experiments carried out by ref 24 at salinities up to 167 g kg⁻¹ and temperatures between 278 and 313 K (not shown are two experiments of ref 24 carried out at salinities of 323 and 325 g kg⁻¹, temperatures of 278 and 313 K, and resulting in $\Delta \varepsilon_{\rm sol}$ of 2.6 and 1.7%, respectively). Panel (B) shows these same simulations in the salinity range between freshwater and seawater (~35 g kg⁻¹) for Ar, Kr, and Xe, compared with experimental observations (salinity dependence functions of this study and ref 14; see Table 2). Experimental data are offset in salinity by 1–2 g kg⁻¹ for visual clarity.

SEIEs in freshwater¹¹ and seawater¹⁴ have shown small, yet statistically significant, salinity dependences of SEIEs in the same sense as the He salinity effect (i.e., a slight increase in $\varepsilon_{\rm sol}$ with increasing salinity).

Precisely quantifying the magnitude of salinity dependences of SEIEs is crucial for the meaningful interpretation of dissolved noble gas isotopes as tracers in seawater 14,15,41 and saline groundwater. 42 Across three classical MD simulations carried out at salinities of 0, 35, and 115 g kg⁻¹ at 298 K (with all other system properties identical; Table 1), we find a salinity effect on SEIEs such that $\varepsilon_{\rm sol}$ increases with salinity for all isotope ratios considered in this study (Figure 6; Table 3). The simulated increases in $\varepsilon_{\rm sol}$ ($\Delta \varepsilon_{\rm sol}$) are consistent in sign with experimental observations, but the magnitude of simulated $\Delta \varepsilon_{\rm sol}$ values is higher than observations for He isotopes, lower than observations for Ar isotopes, and equal (within error) to observations for Kr and Xe isotopes. For example, the simulated $\Delta \varepsilon_{\rm sol}$ value of ${}^{3}{\rm He}/{}^{4}{\rm He}$ of ${\sim}0.6\%$ at \sim 35 g kg⁻¹ salinity (roughly the salinity of seawater) is nearly three times the observed value.²⁴ In both an absolute and relative sense, simulations more closely match experimental observations for salinity dependences of Ar, Kr, and Xe SEIEs, falling within error of $^{86}\mathrm{Kr}/^{82}\mathrm{Kr}$ and $^{136}\mathrm{Xe}/^{129}\mathrm{Xe}$ $\Delta\varepsilon_{\mathrm{sol}}$ observations, while underpredicting the $^{40}\mathrm{Ar}/^{36}\mathrm{Ar}~\Delta\varepsilon_{\mathrm{sol}}$ value by \sim 50% of its overall magnitude at \sim 35 g kg⁻¹ salinity. We suggest that future MD simulation experiments and future experimental determinations to reduce uncertainties may provide a useful opportunity to further evaluate the choice of water model and water-solute interatomic potential functions.

5. DISCUSSION

The close agreement that we observe between simulated and observed SEIEs in this study suggests that a deeper investigation of the simulations may shed light on the fundamental processes driving these isotope effects. Here, we consider the processes and properties that lead to SEIEs within the context of eq. 4, which is derived from the Bigeleisen—Meyer equation. We begin by rearranging eq. 4 (converting α_{sol} to ε_{sol} and approximating $m_h m_l$ as \overline{m}^2) to note that the per-

mass-unit magnitude of a given isotope ratio's SEIE $(\varepsilon_{\rm sol}/\Delta m)$ is proportional to the mean-square force acting on a dissolved noble gas atom $\langle (F)^2 \rangle$ divided by the squared mean atomic mass $(\overline{m})^2$:

$$\frac{\varepsilon_{\rm sol}}{\Delta m} \propto \frac{\langle (F)^2 \rangle}{\overline{m}^2} \tag{11}$$

Thus, starting with experimental observations, we can explore the relative importance of these two potential drivers of SEIEs (i.e., force and mass) by first asking: do observed SEIEs follow an inverse-square relationship with mean atomic mass? If so, this would imply that all dissolved noble gas atoms experience a similar mean-square force.

By comparing $\ln(\varepsilon_{\rm sol}/\Delta m)$ to $\ln(\bar{m})$ for experimentally determined freshwater SEIEs of He, Ne, Ar, Kr, and Xe at 293 K, we find that the data are well explained by a linear trendline with a slope of -1.8 ($R^2 = 0.996$; Figure 7), which is close to the expected slope of -2 for a constant mean-square force (eq 11). However, a closer examination reveals that Ar, Kr, and Xe SEIEs fall along a trendline with a slope of exactly -2.0 ($R^2 =$ 0.998; Figure 7), while Ne and He SEIEs systematically fall below the trendline. Taken together, these observations point to several key physical properties of dissolved noble gas atoms in water. First, the close agreement of experimental SEIEs with the inverse square mass prediction for Ar, Kr, and Xe indicates that the heavier noble gases must indeed experience a virtually identical mean square force acting upon them in a solvation shell. Second, the lighter noble gases (He and Ne), whose SEIEs fall below the inverse square mass prediction, must experience a slightly weaker than expected mean-square force. That is, SEIEs of He and Ne are lower than those predicted for hypothetical Ar, Kr, and Xe atoms of the same mass. Notably, the predicted ${}^{4}\text{He}/{}^{3}\text{He}$ ε_{sol} value based on the Ar–Kr–Xe trendline in Figure 7 is \sim 32.1%, which falls much further from the experimentally known value (16.6%; Table 2) than do the simulated values in freshwater (e.g., ranging from ~19.5 to 22.5% at 298 K; Series # 1, 9, and 11 in Table 3). This indicates that the MD simulations and Dang et al.²³ framework must, at least in part, capture this fundamental shift in $\langle (F)^2 \rangle$

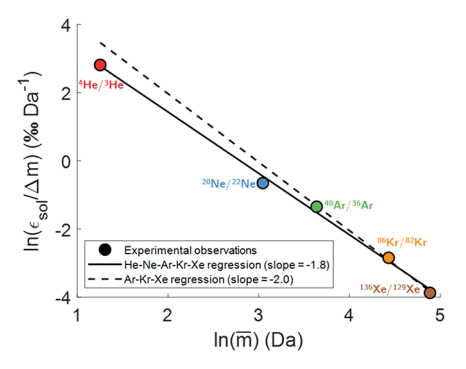


Figure 7. An observed linear relationship between $\ln(\varepsilon_{\rm sol}/\Delta m)$ and $\ln(\overline{m})$ for experimentally observed freshwater SEIEs (at 293 K) indicates that the magnitude of fractionation $(\varepsilon_{\rm sol})$ normalized by the isotopic mass difference (Δm) is generally proportional to the inverse square of the mean isotopic mass (\overline{m}) . Notably, whereas SEIEs for Ar, Kr, and Xe plot along a linear trendline with a slope of -2.0 ($R^2=0.998$), a trendline encompassing all five noble gases has a slope of -1.8 ($R^2=0.996$). This exact inverse-square mass dependence for Ar, Kr, and Xe is consistent with the theoretical expectation for SEIEs (eq 11) provided that all noble gas atoms experience the same mean-square force.

between the light/small (He, Ne) and heavy/large (Ar, Kr, and Xe) noble gases.

Indeed, we find that translational frequencies, $\nu_{\rm et}$ found by MD simulations carried out at different hypothetical noble gas atomic masses yield virtually identical mass-dependent functions for Ar, Kr, and Xe, but they are shifted to lower values for He and Ne (Figure 8). This suggests that, at the

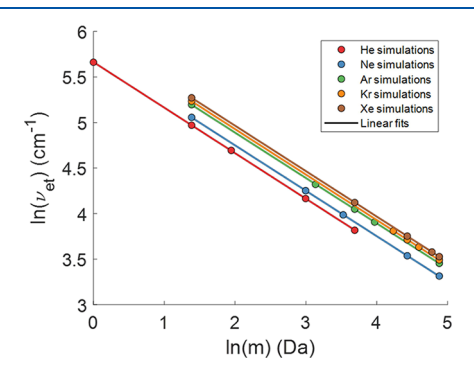


Figure 8. Individual simulation results (markers) and lines of best fit, showing a close linear relationship between $\ln(\nu_{\rm et})$ and $\ln(m)$ for simulations carried out at 298 K for five isotopic masses of each noble gas in freshwater using the SPC/E water model (Series # 1). The slopes of these lines are -0.500, -0.499, -0.498, -0.499, -0.499 for He, Ne, Ar, Kr, and Xe, respectively. We note that virtual identical results (i.e., tight clustering of Ar, Kr, and Xe trendlines, clearly plotting above Ne and He trendlines) were obtained in other simulation series (e.g., implementing the TIP4P water model).

same hypothetical mass, dissolved He and Ne atoms experience a weaker mean-square force acting upon them (and thus a lower rattling frequency) than do Ar, Kr, and Xe atoms, which is consistent with the analysis of experimentally determined SEIEs and their mass dependence (Figure 7).

Why do He and Ne experience a weaker mean-square force acting upon them within a solvation shell? One possibility is that the smaller sizes of He and Ne might allow them to occupy cavities in water without breaking water—water H-bonds, unlike larger Ar, Kr, and Xe atoms. Under this

hypothesis, collisions of He and Ne atoms with water molecules may be softer than those for Ar, Kr, and Xe atoms, which require breaking of H-bonds and formation of a tight cage of water molecules around the solute. Softer collisions would lead to a smaller mean-square force action upon the noble gas atom and a lower rattling frequency. The existence of a solute size threshold that governs H-bond breaking and its impact on the nature of noble gas-water collisions is qualitatively consistent with a hydrophobic solvation theory suggesting a solute size dependence of solvation-free energy, with a threshold size partitioning entropic from enthalpic regimes. 43,44 It is also notable that He and Ne are small enough to have appreciable solubilities in ice, whereas the solubilities of Ar, Kr, and Xe in ice are negligible by comparison. 45,46 An examination of noble gas oxygen radial distribution functions also indicates that He and Ne exhibit broader peaks associated with the first solvation shell than do Ar, Kr, and Xe, consistent with the notion that the smaller noble gases are more loosely held within their solvation shell and likely experience softer collisions (Figures S3 and S4).

The $\ln(\nu_{\rm et}) - \ln(m)$ relationships shown in Figure 8 also suggest that all noble gases (He, Ne, Ar, Kr, and Xe) follow a simple power low whereby translational frequencies are proportional the inverse-square-root of atomic mass (i.e., all trendlines in Figure 8 have a slope very close to -0.5). This suggests that movement of noble gas atoms in water is well described by a simple harmonic oscillator, implying that a solvation shell effectively behaves as an immobile rigid cage with respect to a noble gas atom on the time scale of noble gas rattling. This physical understanding of water behaving in a rigid cage on the characteristic time scale of dissolved noble gas translation is also consistent with the fact that SEIEs can be approximately solely as a function of noble gas mass (Figure 7), as opposed to the reduced mass of a noble gas—water pair.

6. CONCLUSIONS

In this study, we carried out a suite of classical MD simulations and applied the theoretical approach of Dang et al.²³ to compare simulated and experimentally observed SEIEs for the isotopes of He, Ne, Ar, Kr, and Xe in water. We find remarkably close agreement between simulated and observed SEIEs for the heavy noble gases (Ar, Kr, and Xe). Our results suggest that future refinements to experimental determination of SEIEs and their temperature and salinity dependences may provide a useful testbed with which to evaluate and optimize the parameters of classical MD simulations of solutes in water, including the choice of water model and interatomic potential function parametrization. In addition, our results suggest that classical MD simulations may accurately predict equilibrium isotope effects associated with noble gas equilibrium partitioning in other systems, such as dissolution in ice^{45,46} or adsorption on mineral surfaces.^{47–49} We find that both experimentally determined and simulated SEIEs exhibit an exact (or near-exact, in the case of Ne and He) inverse-square mass dependence, suggesting that the mean-square force acting on dissolved noble gas atoms is generally similar, although it appears to be somewhat lower for He and Ne. We hypothesize that the smaller size of the He and Ne atoms may allow them to occupy cavities in water with minimal disturbance to the structure of water, thereby experiencing softer collisions in a more loosely held solvation shell. While the simulations capture the weaker mass dependence of He and Ne SEIEs

suggested by experimental observations, simulated He and Ne SEIEs are still consistently higher than observations. While further work beyond the scope of our study is needed to ascertain the cause of persistent overprediction of He and Ne SEIEs, it is conceivable that some of the data-model disagreement may arise because He and Ne are more sensitive to quantum effects (owing to their lower atomic masses), which are not directly captured by classical MD. However, it is notable that the divergent behavior of He-Ne vs Ar-Kr-Xe is, at least in part, apparent in our classical MD simulations, as the He-Ne vs Ar-Kr-Xe differences in simulated rattling frequencies (Figure 8) are consistent with observation-implied differences in the mean square force acting on a dissolved noble gas (Figure 7). Nonetheless, the poorer He-Ne datamodel agreement may still result from unresolved quantum effects, perhaps implying that higher-order quantum corrections may be required. Future MD simulations that incorporate quantum effects directly (e.g., path integral MD methods $^{50-52}$) may be more successful in simulating He and Ne SEIEs. Alternatively, our results may imply that the interatomic interaction potentials used here yield comparatively less accurate predictions of noble gas-water short-range repulsion (which plays an important role in the solvation of all noble gases) relative to water-water and noble gas-water attractive interactions (which play an increasingly important role in the case of larger noble gases, because of their deeper LJ potential well and their stronger tendency to distort the structure of water). A previous study of Ar VPIEs similarly attributed overprediction of the magnitude of VPIEs to an overly stiff representation of van der Waals repulsion in the LJ potential function.⁵³ We suggest that replacement of the LJ potential with a model that has a weaker exponential dependence for repulsion, such as a modified Buckingham (exp-6) potential, 54,55 may prove fruitful in future efforts to robustly simulate SEIEs of all noble gases.

Taken together, our model data evaluations suggest that the TIP4P model³³ may be most accurate for simulations of simple solutes in water. Further investigation into the influence of water models on the magnitude of kinetic fractionation factors for the noble gases²⁹ (i.e., isotopic differences in diffusivity in water) and for the SEIEs of diatomic gases in water may further enable observational constraints of isotopic fractionation to optimize classical MD simulations of water for other applications. We note that Dang et al.²³ employed an expanded version of the approach used in this study to consider vibration and rotation, in addition to translation, in simulating the SEIE of N₂ in water, finding remarkably close agreement with observations. Future efforts to refine our understanding of SEIEs through experimental determination and classical MD simulation are promising as a means of better understanding fundamental physical processes and optimizing MD simulations for other applications (e.g., simulating systems at temperatures and pressures that are challenging to replicate in a laboratory setting).

ASSOCIATED CONTENT

Data Availability Statement

All processed MD simulation results are included in Tables 3 and S1. Raw simulation output files are available upon request. New experimental determinations of Ar SEIEs in freshwater and saltwater are included as a supplementary data set. The Ar SEIE values in Table 2 are based on these new data.

Solution Supporting Information

The Supporting Information is available free of charge at https://pubs.acs.org/doi/10.1021/acs.jpcb.3c05651.

New Ar isotope SEIE measurements (XLSX) Supplementary figures and table showing additional MD simulation details and results (PDF)

AUTHOR INFORMATION

Corresponding Author

Alan M. Seltzer — Woods Hole Oceanographic Institution, Woods Hole, Massachusetts 02543-1050, United States; orcid.org/0000-0003-2870-1215; Email: aseltzer@whoi.edu

Authors

Sarah A. Shackleton — Department of Geosciences, Princeton University, Princeton, New Jersey 08544, United States

Ian C. Bourg — Department of Civil and Environmental Engineering (CEE) and High Meadows Environmental Institute (HMEI), Princeton University, Princeton, New Jersey 08544, United States; orcid.org/0000-0002-5265-7229

Complete contact information is available at: https://pubs.acs.org/10.1021/acs.jpcb.3c05651

Notes

ı

The authors declare no competing financial interest.

ACKNOWLEDGMENTS

We dedicate this work to Liem X. Dang, whose underappreciated 1989 study on the isotope effects of Henry coefficients in water laid the theoretical foundation for our study. Decades before the first experimental determination of the SEIE of Ar in water, Dang predicted this isotope effect with the correct sign and approximate magnitude (to within 0.7%) using his theory and a 1.25 ps classical MD simulation. Over 30 years later, with the ability to run many orders-ofmagnitude longer simulations, by implementing Dang's thoroughly documented approach, we have been able to accurately simulate equilibrium isotope effects of noble gases in water to compare with new experimental data at the order-0.001% level. We were saddened to learn of Dang's passing several months before we began this work. We hope this paper may serve as a small celebration of Dang's efforts to model a natural phenomenon (that is, SEIEs), presumably driven mostly by intellectual curiosity, without any immediately obvious application at the time. Decades later, his paper has served as a roadmap for our work and, in turn, has helped to solidify our understanding of these quantum effects that underpin new applications of dissolved noble gas isotopes as tracers in the geosciences. In our modern era of impact factors and h-indices, Dang's 1989 paper is a reminder that one's own intellectual curiosity is often reason enough for the pursuit of good science. We are grateful to the National Science Foundation Chemical Oceanography program (award # OCE-2122427) for supporting this work and to the National Energy Research Scientific Computing Center for computational resources. I.C.B. was supported by the U.S. Department of Energy, Office of Science, Office of Basic Energy Sciences, Geosciences Program under Award DE-SC0018419. We thank Bill Jenkins, Dempsey Lott, and Rebecca Tyne for sharing equipment and analytical advice regarding these air-water equilibration experiments, and Jeff Severinghaus for helpful conversations over the past decade about the nature of gas dissolution in water.

REFERENCES

- (1) Kulongoski, J. T.; Hilton, D. R. Applications of Groundwater Helium. In *Advances in Isotope Geochemistry* 2012, 285304.
- (2) Solomon, D. K. 4He in Groundwater. In Environmental Tracers in Subsurface Hydrology; Springer US, 2000; 425–439.
- (3) Schlosser, P.; Stute, M.; Sonntag, C.; Otto Münnich, K. Tritiogenic 3He in Shallow Groundwater. *Earth Planet Sci. Lett.* **1989**, 94 (3–4), 245–256.
- (4) Stute, M.; Sonntag, C.; Deák, J.; Schlosser, P. Helium in Deep Circulating Groundwater in the Great Hungarian Plain: Flow Dynamics and Crustal and Mantle Helium Fluxes. *Geochim. Cosmochim. Acta* 1992, 56 (5), 2051–2067.
- (5) Jenkins, W. J.; Clarke, W. B. The Distribution of 3He in the Western Atlantic Ocean. *Deep Sea Res. Oceanogr. Abstr.* **1976**, 23 (6), 481–494.
- (6) Lupton, J. E.; Craig, H. A Major 3He Source at 15°S on the East Pacific Rise. *Science* **1981**, 214 (4516), 13–18.
- (7) Jenkins, W. J.; Doney, S. C.; Seltzer, A. M.; German, C. R.; Lott, D. E.; Cahill, K. L. A North Pacific Meridional Section (U.S. GEOTRACES GP15) of Helium Isotopes and Noble Gases I: Deep Water Distributions. *Glob. Biogeochem. Cycles* **2023**, 37, No. e2022GB007667, DOI: 10.1029/2022GB007667.
- (8) Stanley, R. H. R.; Jenkins, W. J.; Doney, S. C.; Lott, D. E. The 3 He Flux Gauge in the Sargasso Sea: A Determination of Physical Nutrient Fluxes to the Euphotic Zone at the Bermuda Atlantic Time-Series Site. *Biogeosciences* **2015**, *12* (17), 5199–5210.
- (9) Ng, J.; Tyne, R.; Seltzer, A.; Noyes, C.; McIntosh, J.; Severinghaus, J. A New Large-Volume Equilibration Method for High-Precision Measurements of Dissolved Noble Gas Stable Isotopes. *Rapid Commun. Mass Spectrom.* **2023**, *37* (7), No. e9471.
- (10) Seltzer, A. M.; Bekaert, D. V. A Unified Method for Measuring Noble Gas Isotope Ratios in Air, Water, and Volcanic Gases via Dynamic Mass Spectrometry. *Int. J. Mass Spectrom.* **2022**, 478, No. 116873.
- (11) Seltzer, A. M.; Ng, J.; Severinghaus, J. P. Precise Determination of Ar, Kr and Xe Isotopic Fractionation Due to Diffusion and Dissolution in Fresh Water. *Earth Planet Sci. Lett.* **2019**, *514*, 156–165.
- (12) Seltzer, A. M.; Ng, J.; Danskin, W. R.; Kulongoski, J. T.; Gannon, R. S.; Stute, M.; Severinghaus, J. P. Deglacial Water-Table Decline in Southern California Recorded by Noble Gas Isotopes. *Nat. Commun.* **2019**, *10*, 5739.
- (13) Seltzer, A. M.; Krantz, J. A.; Ng, J.; Danskin, W. R.; Bekaert, D. V.; Barry, P. H.; Kimbrough, D. L.; Kulongoski, J. T.; Severinghaus, J. P. The Triple Argon Isotope Composition of Groundwater on Ten-Thousand-Year Timescales. *Chem. Geol.* **2021**, *583*, No. 120458.
- (14) Seltzer, A. M.; Pavia, F. J.; Ng, J.; Severinghaus, J. P. Heavy Noble Gas Isotopes as New Constraints on the Ventilation of the Deep Ocean. *Geophys. Res. Lett.* **2019**, *46* (15), 84089.
- (15) Seltzer, A. M.; Nicholson, D. P.; Smethie, W. M.; Tyne, R. L.; Le Roy, E.; Stanley, R. H. R.; Stute, M.; Barry, P. H.; McPaul, K.; Davidson, P. W.; et al. Dissolved Gases in the Deep North Atlantic Track Ocean Ventilation Processes. *Proc. Natl. Acad. Sci. U. S. A.* **2023**, *120* (11), No. e2217946120.
- (16) Chialvo, A. A.; Horita, J. Isotopic Effect on Phase Equilibria of Atomic Fluids and Their Mixtures: A Direct Comparison between Molecular Simulation and Experiment. *J. Chem. Phys.* **2003**, *119* (8), 4458.
- (17) Bigeleisen, J.; Phys Lett, A. Statistical Mechanics of Isotope Effects on the Thermodynamic Properties of Condensed Systems. *J. Chem. Phys.* **1961**, 34 (5), 1485–1493.
- (18) Alamre, A.; Badhrees, I.; Death, B.; Licciardi, C.; Sinclair, D. Isotopic Dependence of Vapor Pressure in Xenon. *ACS Omega* **2020**, 5 (45), 28977–28983.

- (19) Lopes, J. N. C.; Pádua, A. A. H.; Rebelo, L. P. N.; Bigeleisen, J. Calculation of Vapor Pressure Isotope Effects in the Rare Gases and Their Mixtures Using an Integral Equation Theory. *J. Chem. Phys.* **2003**, *118* (11), 5028–5037.
- (20) Jancsó, G.; Jancsó, G. Interpretation of Isotope Effects on the Solubility of Gases. *Nukleonika* **2002**, *47*, 53–57.
- (21) Schauble, E. A.; Young, E. D. Mass Dependence of Equilibrium Oxygen Isotope Fractionation in Carbonate, Nitrate, Oxide, Perchlorate, Phosphate, Silicate, and Sulfate Minerals. *Rev. Mineral. Geochem.* **2021**, *86* (1), 137–178.
- (22) Bigeleisen, J.; Mayer, M. G. Statistical Mechanics of Isotopic Systems with Small Quantum Corrections. I. General Considerations and the Rule of the Geometric Mean. *Paleotemperature Scale. J. Chem. Phys.* 1947, 15 (5), 261.
- (23) Dang, L. X.; Bopp, P.; Wolfsberg, M. Evaluation of Isotope Effects on Henry's Law Constants by a Molecular Dynamics Technique. Z. Naturforsch. Sect. A J. Phys. Sci. 1989, 44 (5), 485–491.
- (24) Benson, B. B.; Krause, D. Isotopic Fractionation of Helium during Solution: A Probe for the Liquid State. *J. Solution Chem.* **1980**, 9 (12), 895–909.
- (25) Weiss, R. F. Helium Isotope Effect in Solution in Water and Seawater. *Science* 1970, 168 (3928), 247-248.
- (26) Tempest, K. E.; Emerson, S. Kinetic Isotopic Fractionation of Argon and Neon during Air-Water Gas Transfer. *Mar. Chem.* **2013**, 153, 39–47.
- (27) Plimpton, S. Fast Parallel Algorithms for Short-Range Molecular Dynamics. *J. Comput. Phys.* **1995**, *117* (1), 1–19.
- (28) Berendsen, H. J. C.; Grigera, J. R.; Straatsma, T. P. The Missing Term in Effective Pair Potentials. *J. Phys. Chem.* **1987**, *91* (24), 6269–6271.
- (29) Bourg, I. C.; Sposito, G. Isotopic Fractionation of Noble Gases by Diffusion in Liquid Water: Molecular Dynamics Simulations and Hydrologic Applications. *Geochim. Cosmochim. Acta* **2008**, 72 (9), 2237–2247.
- (30) Vega, C.; Abascal, J. L. F. Simulating Water with Rigid Non-Polarizable Models: A General Perspective. *Phys. Chem. Chem. Phys.* **2011**, *13* (44), 19663–19688.
- (31) Hura, G.; Russo, D.; Glaeser, R. M.; Head-Gordon, T.; Krack, M.; Parrinello, M. Water Structure as a Function of Temperature from X-Ray Scattering Experiments and Ab Initio Molecular Dynamics. *Phys. Chem. Chem. Phys.* **2003**, *5* (10), 1981–1991.
- (32) Gadikota, G.; Dazas, B.; Rother, G.; Cheshire, M. C.; Bourg, I. C. Hydrophobic Solvation of Gases (CO2, CH4, H2, Noble Gases) in Clay Interlayer Nanopores. *J. Phys. Chem. C* **2017**, *121* (47), 26539–26550
- (33) Jorgensen, W. L.; Chandrasekhar, J.; Madura, J. D.; Impey, R. W.; Klein, M. L. Comparison of Simple Potential Functions for Simulating Liquid Water. *J. Chem. Phys.* **1983**, 79 (2), 926–935.
- (34) Abascal, J. L. F.; Sanz, E.; Fernández, R. G.; Vega, C. A Potential Model for the Study of Ices and Amorphous Water: TIP4P/ Ice. J. Chem. Phys. 2005, 122 (23), 234511.
- (35) Warr, O.; Ballentine, C. J.; Mu, J.; Masters, A. Optimizing Noble Gas-Water Interactions via Monte Carlo Simulations. *J. Phys. Chem. B* **2015**, *119* (45), 14486–14495.
- (36) Verlet, L. Computer "Experiments" on Classical Fluids. I. Thermodynamical Properties of Lennard-Jones Molecules. *Phys. Rev.* **1967**, *159* (1), 98.
- (37) Smith, D. E.; Dang, L. X. Computer Simulations of NaCl Association in Polarizable Water. *J. Chem. Phys.* **1994**, *100* (5), 3757–3766
- (38) Jenkins, W. J.; Lott, D. E.; Cahill, K. L. A Determination of Atmospheric Helium, Neon, Argon, Krypton, and Xenon Solubility Concentrations in Water and Seawater. *Mar. Chem.* **2019**, *211*, 94–107.
- (39) Hamme, R. C.; Emerson, S. R. The Solubility of Neon, Nitrogen and Argon in Distilled Water and Seawater. *Deep Sea Res. 1 Oceanogr. Res. Pap.* **2004**, *51* (11), 1517–1528.

- (40) Setschenow, J. Über Die Konstitution Der Salzlösungen Auf Grund Ihres Verhaltens Zu Kohlensäure. Z. Phys. Chem. 1889, 4U, 1.
- (41) Nicholson, D.; Emerson, S.; Caillon, N.; Jouzel, J.; Hamme, R. C. Constraining Ventilation during Deepwater Formation Using Deep Ocean Measurements of the Dissolved Gas Ratios 40 Ar/ 36 Ar, N 2/Ar, and Kr/Ar. *J. Geophys. Res.* **2010**, *115* (C11), C11015.
- (42) Kipfer, R.; Aeschbach-Hertig, W.; Peeters, F.; Stute, M. Noble Gases in Lakes and Ground Waters. *Rev. Mineral. Geochem.* **2002**, 47 (1), 615–700.
- (43) Huang, D. M.; Geissler, P. L.; Chandler, D. Scaling of Hydrophobic Solvation Free Energies. *J. Phys. Chem. B* **2001**, *105* (28), 6704–6709.
- (44) Chandler, D. Interfaces and the Driving Force of Hydrophobic Assembly. *Nature* **2005**, 437 (7059), 640–647.
- (45) Top, Z.; Martin, S.; Becker, P. A Laboratory Study of Dissolved Noble Gas Anomaly Due to Ice Formation. *Geophys. Res. Lett.* **1988**, 15 (8), 796–799.
- (46) Hood, E. M.; Howes, B. L.; Jenkins, W. J. Dissolved Gas Dynamics in Perennially Ice-Covered Lake Fryxell, Antarctica. *Limnol. Oceanogr.* **1998**, 43 (2), 265–272.
- (47) Torgersen, T.; Kennedy, B. M.; van Soest, M. C. Diffusive Separation of Noble Gases and Noble Gas Abundance Patterns in Sedimentary Rocks. *Earth Planet Sci. Lett.* **2004**, 226 (3–4), 477–489.
- (48) Jackson, C. R. M.; Parman, S. W.; Kelley, S. P.; Cooper, R. F. Noble Gas Transport into the Mantle Facilitated by High Solubility in Amphibole. *Nat. Geosci.* **2013**, *6* (7), 562–565.
- (49) Derkowski, A.; Szczerba, M.; Środoń, J.; Banaś, M. Radiogenic Ar Retention in Residual Silica from Acid-Treated Micas. *Geochim. Cosmochim. Acta* **2014**, 128, 236–248.
- (50) Blanchard, M.; Balan, E.; Schauble, E. A. Equilibrium Fractionation of Non-Traditional Isotopes: A Molecular Modeling Perspective. *Rev. Mineral. Geochem.* **2017**, *82*, 27–63.
- (51) Lobaugh, J.; Voth, G. A. A Quantum Model for Water: Equilibrium and Dynamical Properties. *J. Chem. Phys.* **1997**, *106* (6), 2400–2410.
- (52) Guillot, B.; Guissani, Y. Quantum Effects in Simulated Water by the Feynman-Hibbs Approach. *J. Chem. Phys.* **1998**, *108* (24), 10162–10174.
- (53) Casanova, G.; Levi, A.; Terzi, N. Mean Square Force in Liquid Argon and Separation Factor of Isotopes. *Physica* **1964**, *30* (5), 937–947.
- (54) Cao, Z.; Tester, J. W.; Sparks, K. A.; Trout, B. L. Molecular Computations Using Robust Hydrocarbon-Water Potentials for Predicting Gas Hydrate Phase Equilibria. *J. Phys. Chem. B* **2001**, 105 (44), 10950–10960.
- (55) Mason, E. A. Transport Properties of Gases Obeying a Modified Buckingham (Exp-Six) Potential. *J. Chem. Phys.* **1954**, 22 (2), 169–186.